ISSN 1674-1056
http://cpb.iphy.ac.cn
http://iopscience.iop.org/cpb
中国物理 B
Chinese Physics
中国物理 Chinese Physics B

Optimal phase estimation with photon-number difference measurement using twin-Fock states of light

J H Xu(徐佳慧)[1], J Z Wang(王建中)[1], A X Chen(陈爱喜)[1], Y Li(李勇)[2], G R Jin(金光日)[1]
Citation: Chin. Phys. B . 2019, 28(12): 120303 . **doi:** 10.1088/1674-1056/ab4e7f
Journal homepage: http://cpb.iphy.ac.cn; http://iopscience.iop.org/cpb

What follows is a list of articles you may be interested in

Influence of homodyne-based feedback control on the entropic uncertainty in open quantum system

Juju Hu(胡菊菊), Qin Xue(薛琴)
Chin. Phys. B . 2019, 28(7): 070303 . **doi:** 10.1088/1674-1056/28/7/070303

Atom interferometers with weak-measurement path detectors and their quantum mechanical analysis

Zhi-Yuan Li(李志远)
Chin. Phys. B . 2019, 28(6): 060301 . **doi:** 10.1088/1674-1056/28/6/060301

Dynamical control of population and entanglement for open Λ-type atoms by engineering the environment

Xiao-Lan Wang(王晓岚), Yu-Kun Ren(任玉坤), Hao-Sheng Zeng(曾浩生)
Chin. Phys. B . 2019, 28(3): 030301 . **doi:** 10.1088/1674-1056/28/3/030301

Controlling of entropic uncertainty in open quantum system via proper placement of quantum register

Ying-Hua Ji(嵇英华), Qiang Ke(柯强), Ju-Ju Hu(胡菊菊)
Chin. Phys. B . 2018, 27(10): 100302 . **doi:** 10.1088/1674-1056/27/10/100302

Quantum uncertainty relations of quantum coherence and dynamics under amplitude damping channel

Fugang Zhang(张福刚), Yongming Li(李永明)
Chin. Phys. B . 2018, 27(9): 090301 . **doi:** 10.1088/1674-1056/27/9/090301

Optimal phase estimation with photon-number difference measurement using twin-Fock states of light*

J H Xu(徐佳慧)[1], J Z Wang(王建中)[1], A X Chen(陈爱喜)[1], Y Li(李勇)[2], and G R Jin(金光日)[1,†]

[1] *Key Laboratory of Optical Field Manipulation of Zhejiang Province and Physics Department of Zhejiang Sci-Tech University, Hangzhou* 310018, *China*
[2] *Beijing Computational Science Research Center, Beijing* 100193, *China*

(Received 5 August 2019; revised manuscript received 24 September 2019; published online 29 November 2019)

Quantum phase measurement with multiphoton twin-Fock states has been shown to be optimal for detecting equal numbers of photons at the output ports of a Mach–Zehnder interferometer (i.e., the so-called single-fringe detection), since the phase sensitivity can saturate the quantum Cramér–Rao lower bound at certain values of phase shift. Here we report a further step to achieve a global phase estimation at the Heisenberg limit by detecting the particle-number difference (i.e., the $\hat{J}_z$ measurement). We show the role of experimental imperfections on the ultimate estimation precision with the six-photon twin-Fock state of light. Our results show that both the precision and the sensing region of the $\hat{J}_z$ measurement are better than those of the single-fringe detection, due to combined contributions of the measurement outcomes. We numerically simulate the phase estimation protocol using an asymptotically unbiased maximum likelihood estimator.

Keywords: foundations of quantum mechanics, measurement theory, nonclassical interferometry

PACS: 03.65.Ta, 42.50.St **DOI:** 10.1088/1674-1056/ab4e7f

1. Introduction

Optimal measurement scheme with a proper choice of data processing is important to realize high-precision phase measurement.[1–3] For the commonly used particle-number difference measurement (or the $\hat{J}_z$ measurement) over quasi-classical coherent states, the phase sensitivity is constrained by the shot-noise limit (SNL) $\delta\theta \sim O(1/\sqrt{N})$, where N is the number of particles of the input state. Various schemes have been proposed and demonstrated to improve the phase estimation precision beyond the SNL by using quantum entangled states,[4,5] e.g., the so-called NOON states $(|N,0\rangle_{a,b} + |0,N\rangle_{a,b})/\sqrt{2}$. This is a maximally entangled state with all the particles being either in the mode a or in the mode b, leading to the Heisenberg limited phase sensitivity $\delta\theta = 1/N$.[3–6] However, the NOON states are difficult to prepare and are easily subject to the loss-induced decoherence.[7,8]

Compared with various kinds of entangled states, the twin-Fock states of photons (or atoms) $|n,n\rangle_{a,b}$ are believed to be more robust to the decoherence and hence result in a better phase estimation precision under typical experimental noise.[9] With the twin-Fock states as the input of the Mach–Zehnder interferometer (MZI), the interferometric signal is vanishing if one performs the $\hat{J}_z$ measurement at the output ports.[10] Therefore, various measurement schemes such as the parity detection,[11–17] the $\hat{J}_z^2$ measurement,[18–20] and the so-called single-fringe detection[21] have been proposed to realize high-precision phase measurement beyond the SNL. These phase estimation protocols are based on the inversion estimators with their uncertainties predicted by the error-propagation formula.

According to the general theory of quantum metrology, the ultimate estimation precision is determined by the Cramér–Rao lower bound (CRB)[22–25] $\delta\theta_{\rm CRB} = 1/\sqrt{\mathcal{F}(\theta)}$, where $\mathcal{F}(\theta)$ is the classical Fisher information (CFI), dependent on the measurement probabilities. Furthermore, the CRB can be saturated asymptotically by maximum likelihood estimation (MLE) or Bayesian estimation.[26,27] In this paper, we investigate high-precision phase measurement with the twin-Fock states of light. We show that the $\hat{J}_z$ measurement is optimal to achieve a global phase estimation at the Heisenberg limit. More specially, we find that the CRB saturates the quantum Cramér–Rao lower bound (QCRB) for any value of the phase shift, i.e., $\delta\theta_{\rm CRB} = \delta\theta_{\rm QCRB} = 1/\sqrt{F_{\rm Q}} \sim O(1/N)$, where $N = 2n$ is the number of particles and $F_{\rm Q} = N(N+2)/2$ denotes the quantum Fisher information (QFI). This result remains valid for the $\hat{J}_z^2$ measurement. To demonstrate it clearly, we use the six-photon twin-Fock state as the input and consider experimental imperfections in the measurement probabilities, similar to a recent experimental work.[21] Our results indicate that both the precision and the sensing region of the $\hat{J}_z$ measurement are better than those of the single-fringe measurement. Finally, we numerically simulate the phase estimation protocol using the asymptotically unbiased maximum likelihood estimator.

*Project supported by the National Natural Science Foundation of China (Grant Nos. 91636108, 11775190, and 11774024), Science Foundation of Zhejiang Sci-Tech University, China (Grant No. 18062145-Y), Open Foundation of Key Laboratory of Optical Field Manipulation of Zhejiang Province, China (Grant No. ZJOFM-2019-002), and Science Challenge Project, China (Grant No. TZ2018003).

†Corresponding author. E-mail: grjin@zstu.edu.cn

© 2019 Chinese Physical Society and IOP Publishing Ltd

2. Fisher information of particle-number difference measurement

For the input twin-Fock states $|n,n\rangle_{a,b}$, the probabilities for detecting particle-number difference (i.e., the so-called $\hat{J}_z$ measurement) are given by

$$p_\mu(\theta)=\left|\langle j,\mu|\,\mathrm{e}^{-\mathrm{i}\theta\hat{J}_y}\,|j,0\rangle\right|^2=\left[d^j_{\mu,0}(\theta)\right]^2, \tag{1}$$

conditioned on a phase shift θ. For brevity, we have introduced Schwinger's representation of the angular momentum $\hat{J}\equiv(\hat{J}_x,\hat{J}_y,\hat{J}_z)=\frac{1}{2}(\hat{a}^\dagger,\hat{b}^\dagger)\hat{\sigma}\binom{\hat{a}}{\hat{b}}$, where $\hat{a}$ and $\hat{b}$ denote two bosonic modes and $\hat{\sigma}=(\hat{\sigma}_x,\hat{\sigma}_y,\hat{\sigma}_z)$ is the Pauli matrix. The unitary operator $\exp(-\mathrm{i}\theta\hat{J}_y)$ represents a sequence of actions of the 50 : 50 beamsplitter at the output port, the phase accumulation at the two paths, and the 50 : 50 beamsplitter at the input port.[26,28] In Eq. (1), the Wigner's d-matrix elements are defined as usual (see e.g., Ref. [29]), $d^j_{\mu,\mu'}(\theta)\equiv\langle j,\mu|\exp(-\mathrm{i}\theta\hat{J}_y)|j,\mu'\rangle\in\mathbb{R}$. Hereinafter, $|j,\mu\rangle\equiv|n,N-n\rangle_{a,b}$ denote the eigenstates of $\hat{J}_z$, with $\mu=n-j\in[-j,+j]$ and $j=N/2$, representing n particles in the a-mode and $N-n$ particles in the b-mode. As a result, the input twin-Fock states can be expressed as $|j,\mu\rangle$ with $\mu=0$ and hence the output state $|\psi(\theta)\rangle=\exp(-\mathrm{i}\theta\hat{J}_y)|j,0\rangle$. In Fig. 1, we show the phase-dependence of $\{p_\mu(\theta)\}$ for the six-particle twin-Fock state (i.e., $N=6$), which satisfies $p_\mu(-\theta)=p_\mu(\theta)$ and $p_{-\mu}(\theta)=p_\mu(\theta)$. As depicted by the red dashed lines, one can easily see that the probabilities $p_0(\theta)$ and $p_{\pm1}(\theta)$ exhibit 6-fold oscillatory patterns.

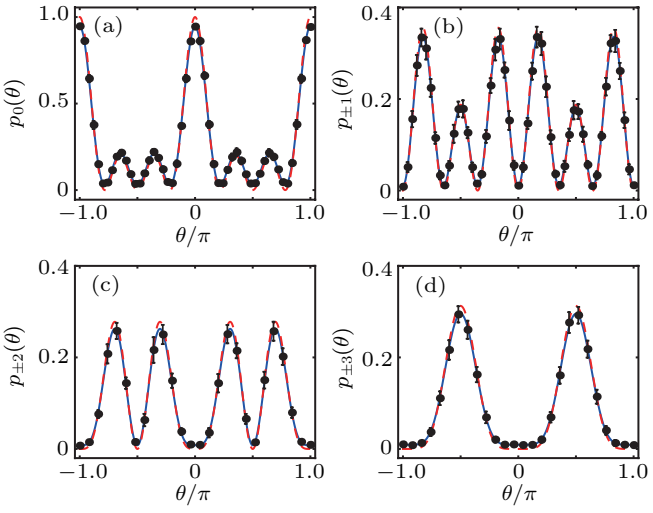


Fig. 1. The conditional probabilities for detecting particle-number difference: $p_\mu(\theta)$ for (a) $\mu=0$, (b) $\mu=\pm1$, (c) $\mu=\pm2$, and (d) $\mu=\pm3$. The red dashed lines show the ideal results; the blue solid lines give the occurrence probabilities with the experimental imperfections, obtained from Eq. (6). Numerical simulations give the statistical average of the occurrence frequency $\langle\mathcal{N}^{(i)}_\mu\rangle_\mathrm{s}/\mathcal{N}$ (the solid circles) and its standard derivation (the bars) of each outcome, simulated by $M=20$ replicas of $\mathcal{N}=500$ random numbers at each $\theta\in(-\pi,\pi)$. Hereinafter, $\langle A^{(i)}\rangle_\mathrm{s}=\sum_{i=1}^M A^{(i)}/M$ denotes the statistical average.

The amount of phase information that is encoded by an arbitrary pure state $|\psi(\theta)\rangle=\exp(-\mathrm{i}\theta\hat{J}_y)|\psi_\mathrm{in}\rangle$ is given by the quantum Fisher information $F_\mathrm{Q}=4[\langle\hat{J}_y^2\rangle_\mathrm{in}-\langle\hat{J}_y\rangle^2_\mathrm{in}]$, where the expectation value $\langle\cdots\rangle_\mathrm{in}$ is taken with respect to the input state. For the N-photon twin-Fock states, it is easy to obtain the QFI $F_\mathrm{Q}=4\langle\hat{J}_y^2\rangle_\mathrm{in}=N(N+2)/2$ and hence the QCRB $\delta\theta_\mathrm{QCRB}=1/\sqrt{F_\mathrm{Q}}\simeq\sqrt{2}/N$. To saturate it, we consider the $\hat{J}_z$ measurement and calculate the CFI[22–25]

$$\begin{aligned}\mathcal{F}(\theta)&=\sum_{\mu=-j}^{+j}p_\mu(\theta)\left[\frac{\partial\ln p_\mu(\theta)}{\partial\theta}\right]^2\\&=\sum_{\mu=-j}^{+j}\frac{1}{p_\mu(\theta)}\left[\frac{\partial p_\mu(\theta)}{\partial\theta}\right]^2,\end{aligned} \tag{2}$$

which determines the CRB $\delta\theta_\mathrm{CRB}=1/\sqrt{\mathcal{F}(\theta)}$. The occurrence probabilities $\{p_\mu(\theta)\}$ have been defined by Eq. (1), satisfying

$$\frac{\partial p_\mu(\theta)}{\partial\theta}=2\sqrt{p_\mu(\theta)}\langle j,\mu|\,\mathrm{e}^{-\mathrm{i}\theta\hat{J}_y}(-\mathrm{i}\hat{J}_y)|j,0\rangle. \tag{3}$$

Similar to Refs. [30] and [31], one can note that the first-order derivations of the d-matrix elements $\partial d^j_{\mu,0}(\theta)/\partial\theta=\langle j,\mu|\exp(-\mathrm{i}\theta\hat{J}_y)(-\mathrm{i}\hat{J}_y)|j,0\rangle$ are real, which simplify the CFI as

$$\mathcal{F}(\theta)=4\langle j,0|\hat{J}_y^2|j,0\rangle=\frac{N(N+2)}{2}=F_\mathrm{Q}, \tag{4}$$

where we have used the completeness condition $\sum_\mu|j,\mu\rangle\langle j,\mu|=1$. For the 6-particle twin-Fock state, one can obtain the ideal result of the CFI $\mathcal{F}(\theta)=F_\mathrm{Q}=24$ (see the upper horizontal line of Fig. 2), independent of θ. The above results indicate that the $\hat{J}_z$ measurement is optimal for the N-particle twin-Fock states due to $\delta\theta_\mathrm{CRB}=\delta\theta_\mathrm{QCRB}\sim O(1/N)$, which holds for an arbitrary phase shift $\theta\in(-\pi,\pi)$. Such a Heisenberg limited phase sensitivity can be saturated by the maximum likelihood estimation (see below).

For the twin-Fock input states, the output signal of the $\hat{J}_z$ measurement is always vanishing,[32] implying that the inversion estimator based on the average signal cannot infer the true value of the phase shift. To overcome it, other measurement schemes have been proposed, e.g., the parity measurement[11–17] and the $\hat{J}_z^2$ measurement.[18–20] With the error propagation formula, it has been shown that the phase sensitivity of the two measurements can only saturate the QCRB at a certain value of the phase shift (e.g., $\theta=0$).[21] We show that the CFI of the $\hat{J}_z^2$ measurement is the same with that of the $\hat{J}_z$ measurement, leading to a global phase estimation $\delta\theta_\mathrm{CRB}=\delta\theta_\mathrm{QCRB}\simeq\sqrt{2}/N$ (see Appendix A).

Recently, Xiang *et al.*[21] have demonstrated a very simple and efficient single-fringe detection. Their measurement scheme has been proposed originally by Sun *et al.*[33] and is equivalently to a projection measurement $\hat{\Pi}=|j,0\rangle\langle j,0|$ over the output state, with the signal $\langle\hat{\Pi}\rangle=\langle\psi(\theta)|\hat{\Pi}|\psi(\theta)\rangle=p_0(\theta)$, corresponding to Eq. (1) for $\mu=0$. Note that $p_0(\theta)$ describes the occurrence probability for detecting equal numbers of particles at the two output ports $n_1=n_2=n$, i.e.,

$\mu = (n_1 - n_2)/2 = 0$, denoted hereafter by the outcome "0". All the other detection events can be treated as a single outcome "$\emptyset$", with the occurrence probability $p_\emptyset(\theta) = 1 - p_0(\theta)$.

Obviously, the single-fringe detection is indeed a binary-outcome measurement scheme,[34–36] where the two outcomes "0" and "$\emptyset$" can be obtained by coarse-graining over the original $(N+1)$ measurement outcomes of the $\hat{J}_z$ measurement. For any binary-outcome measurement, it has been shown that the inversion estimator based on the average signal always saturates the CRB $\delta\theta_{\rm CRB} = 1/\sqrt{\mathcal{F}_{\rm bin}(\theta)}$,[34–36] with the CFI given by

$$\mathcal{F}_{\rm bin}(\theta) = \frac{[p_0'(\theta)]^2}{p_0(\theta)} + \frac{[p_\emptyset'(\theta)]^2}{p_\emptyset(\theta)} = \frac{[p_0'(\theta)]^2}{p_0(\theta)p_\emptyset(\theta)}, \tag{5}$$

where $p_k'(\theta) = \partial p_k(\theta)/\partial\theta$. Using such a simple measurement scheme, Xiang *et al.*[21] have shown that the achievable phase sensitivity can saturate the QCRB at the optimal working points (e.g., $\theta = 0$) due to $\mathcal{F}_{\rm bin}(0) = F_{\rm Q} = 24$. However, the role of the experimental imperfections reduces this ideal result, also introducing a phase-dependent Fisher information.[21]

3. Experimental imperfections

The experimental imperfections can be taken into account artificially.[37] Similar to Ref. [38], we adopt a simple method by introducing the peak heights and the visibility in the probabilities $\{p_\mu(\theta)\}$, i.e., replacing the occurrence probabilities by

$$p_\mu^{(\rm im)}(\theta) = A_0 p_\mu(\theta) + B_\mu, \tag{6}$$

where we have introduced the θ-independent parameters $A_0 = 0.9293$, $B_0 = 0.0245$, $B_1 = 0.0087$, $B_2 = 0.0068$, and $B_3 = 0.0076$ (see Appendix B). For brevity, we still assume $p_{-\mu}^{(\rm im)}(\theta) = p_{+\mu}^{(\rm im)}(\theta)$, which requires $B_{-\mu} = B_{+\mu}$. The above treatments ensure the normalization condition $\sum_\mu p_\mu^{(\rm im)}(\theta) = \sum_\mu p_\mu(\theta) = 1$. In Fig. 1, we plot the occurrence probabilities $p_\mu^{(\rm im)}(\theta)$ as a function of θ (the solid blue lines), which also exhibits a multi-fold oscillatory pattern, but with the visibility less than that of the ideal results $p_\mu(\theta)$. For instance, as shown in Fig. 1(a), we find that the visibility of $p_0^{(\rm im)}(\theta)$ is about 94%, consistent with the experimental result of Ref. [21].

To simulate the $\hat{J}_z$ measurement, we first generate $\mathcal{N}$ random numbers according to $\{p_\mu^{(\rm im)}(\theta)\}$ at a given phase shift (see Appendix B). The occurrence numbers of all the outcomes $\{\mathcal{N}_\mu\}$ and hence the occurrence frequencies can be obtained from the $\mathcal{N}$ random numbers, which comprise a single phase measurement.[27] Next, we repeat the above process to obtain the average occurrence frequencies (see the circles of Fig. 1) for any value of $\theta \in (-\pi, \pi)$, which can be fitted by $p_\mu^{(\rm fit)}(\theta) \approx p_\mu^{(\rm im)}(\theta)$. In a real experiment, the phase-dependent occurrence probabilities can be obtained from the interferometer calibration.

Using the occurrence probabilities $\{p_\mu^{(\rm im)}(\theta)\}$, we obtain the CFI of the $\hat{J}_z$ measurement $\mathcal{F}(\theta)$ and that of the single-fringe detection $\mathcal{F}_{\rm bin}(\theta)$, as depicted by Fig. 2. One can see that both $\mathcal{F}(\theta)$ and $\mathcal{F}_{\rm bin}(\theta)$ cannot reach the ideal result of the QFI $F_{\rm Q} = 24$. For the single-fringe detection (see the thin solid line), the phase-dependence of $\mathcal{F}_{\rm bin}(\theta)$ shows a quite good agreement with that of Ref. [21]. Maximum of the CFI is found at the optimal working point $\theta_{\max} = 0.29$ (16.5°), with $\mathcal{F}_{\rm bin,max} \equiv \mathcal{F}_{\rm bin}(\theta_{\max}) = 19.4$. While for the $\hat{J}_z$ measurement (the solid thick line), $\mathcal{F}_{\max} \equiv \mathcal{F}(\theta_{\max}) = 20.1$ appears at $\theta_{\max} = 0.35$ (20°).

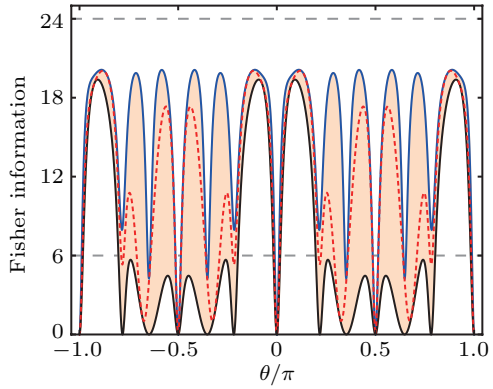


Fig. 2. The CFI for the $\hat{J}_z$ measurement (thick solid line), the single-fringe detection (thin solid line), and the multi-fringe detection (red dashed line), obtained respectively, from Eqs. (2), (5), and (7), with $\{p_\mu^{(\rm im)}(\theta)\}$. The dashed horizontal lines are the classical limit of the QFI $F_{\rm Q} = N$ and the ideal result of the QFI with the twin-Fock input state $F_{\rm Q} = N(N+2)/2$ for $N = 6$. The shaded area is a region where the CFI of the $\hat{J}_z$ measurement outperforms that of the single-fringe detection.

The shaded area in Fig. 2 is a region where the amount of phase information extracted by the $\hat{J}_z$ measurement is larger than that of the single-fringe detection. Obviously, this is straightforward since the former one contains $(N+1)$ measurement contributions and hence $\mathcal{F}_{\max} > \mathcal{F}_{\rm bin,max}$. However, to find out which measurement outcomes dominate in the CFI is still nontrivial. We now consider the CFI of a multi-outcome measurement, where besides the outcome $\mu = 0$, additional contributions from the outcomes $\mu = \pm 2$ are taken into account,

$$\mathcal{F}_{\rm mul}(\theta) = \frac{[p_0'(\theta)]^2}{p_0(\theta)} + 2\frac{[p_2'(\theta)]^2}{p_2(\theta)} + \frac{[p_\emptyset'(\theta)]^2}{p_\emptyset(\theta)}. \tag{7}$$

Here, the factor 2 in the second term comes from the symmetry property $p_{-2}(\theta) = p_2(\theta)$. Note that all the other outcomes with $\mu = \pm 1, \pm 3$ have been treated as a single outcome "$\emptyset$", with the occurrence probability $p_\emptyset(\theta) = 1 - p_0(\theta) - 2p_2(\theta)$.

Compared with the single-fringe case, $\mathcal{F}_{\rm mul}(\theta)$ is indeed the CFI of a multi-fringe detection.[36] Using the occurrence probabilities $\{p_\mu^{(\rm im)}(\theta)\}$, we calculate the phase-dependence of $\mathcal{F}_{\rm mul}(\theta)$, as illustrated by the red dashed line of Fig. 2. One can see that the maximum of $\mathcal{F}_{\rm mul}(\theta)$ also appears at

$\theta_{\max} = 0.35$ (20°), with $\mathcal{F}_{\mathrm{mul,max}} \equiv \mathcal{F}_{\mathrm{mul}}(\theta_{\max}) > \mathcal{F}_{\mathrm{bin,max}}$. Obviously, both $\mathcal{F}_{\mathrm{bin}}(\theta)$ and $\mathcal{F}_{\mathrm{mul}}(\theta)$ are obtained by coarse-graining over the original $(N+1)$ measurement outcomes, leading to $\mathcal{F}_{\mathrm{bin}}(\theta) < \mathcal{F}_{\mathrm{mul}}(\theta) \lesssim \mathcal{F}(\theta)$. Indeed, the coarse-graining method over a general multi-outcome measurement (i.e., combining several different outcomes into a single measurement outcome) will reduce the CFI; see Appendix C. Our results in Fig. 2 show that the outcomes $\mu = 0, \pm 2$ are of importance to achieve the best sensitivity of the $\hat{J}_z$ measurement $\mathcal{F}_{\max} \gtrsim \mathcal{F}_{\mathrm{mul,max}} > \mathcal{F}_{\mathrm{bin,max}}$.

4. Maximum likelihood estimation

To saturate the CRB, we consider the well-known phase-estimation protocol based on the MLE, which is unbiased as the number of independent measurements $\mathcal{N} \gg 1$ (see e.g. Ref. [22]). Numerically, the MLE θ_{est} can be solved by maximizing the likelihood function (i.e., a multinomial distribution)

$$\mathcal{P}(\theta|\{\mathcal{N}_\mu\}) = \mathcal{N}! \prod_{\mu=-j}^{+j} \frac{1}{\mathcal{N}_\mu!} \left[p_\mu^{(\mathrm{fit})}(\theta)\right]^{\mathcal{N}_\mu}, \tag{8}$$

where $\mathcal{N}_\mu = \mathcal{N}_\mu(\theta_0)$ denotes the occurrence number of each outcome μ at a given true value of phase shift θ_0, and $p_\mu^{(\mathrm{fit})}(\theta)$ is a fit of the averaged occurrence frequency of each outcome (see Appendix B). Hereinafter, we directly use $\{p_\mu^{(\mathrm{im})}(\theta)\}$ to speed up numerical simulations.

In Fig. 3, we plot the scaled phase distribution $\mathcal{P}(\theta|\{\mathcal{N}_\mu\})$ as a function of θ for $\theta_0 = \pi/4$. From the inset, one can see that there are four peaks of $\mathcal{P}(\theta|\{\mathcal{N}_\mu\})$ over the entire phase interval $\theta \in (-\pi, \pi)$, and only one of them can be used to predict θ_0. This leads to the so-called phase ambiguity.[39–41] To avoid it, we simply introduce a prior knowledge about θ_0 using the phase distribution $P(\theta)\mathcal{P}(\theta|\{\mathcal{N}_\mu\})$, where $P(\theta) = 1$ for $\theta \in (0, \pi/2)$, and 0 outside. For large enough $\mathcal{N}$, one can find that the phase distribution can be well approximated by a Gaussian with respect to the phase shift θ,

$$\mathcal{P}(\theta|\{\mathcal{N}_\mu\}) \propto \exp\left[-\frac{(\theta-\theta_{\mathrm{est}})^2}{2\sigma^2}\right], \tag{9}$$

where σ is 68.3% confidence interval of the Gaussian around the MLE,[38] and determined by

$$\sigma \approx \sqrt{\frac{1}{\left|\partial^2 \mathcal{P}(\theta|\{\mathcal{N}_\mu\})/\partial\theta^2\right|}}. \tag{10}$$

In Fig. 4, we plot the statistical average of the phase uncertainty $\sqrt{\mathcal{N}}\sigma$ (see the circles) and its standard derivation (the bars) for each true value of phase shift $\theta_0 \in (0, \pi/2)$. From the inset, one can note that the standard derivation of the MLE $\gg (\theta_0 - \langle\theta_{\mathrm{est}}\rangle_{\mathrm{s}})$, indicating that the MLE is unbiased.[27] As a result, the phase uncertainty per measurement shows a good agreement with the CRB $1/\sqrt{\mathcal{F}(\theta)}$, see the blue solid line. Remarkably, the CRB of the $\hat{J}_z$ measurement can beat the shot-noise limit within a phase interval, e.g., $0 < \theta_0 < \arctan 2$ ($\sim 63°$); while for the single-fringe detection, it is the interval $0 < \theta_0 < \arctan\sqrt{2/3}$ ($\sim 39°$). This means that the quantum-enhancement sensing region of the $\hat{J}_z$ measurement is about twice wider than that of the single-fringe detection (see the vertical grid lines of Fig. 4). The enlarged sensing region is important in quantum multiparticle microscopy that uses non-classical states of light for illumination.[42]

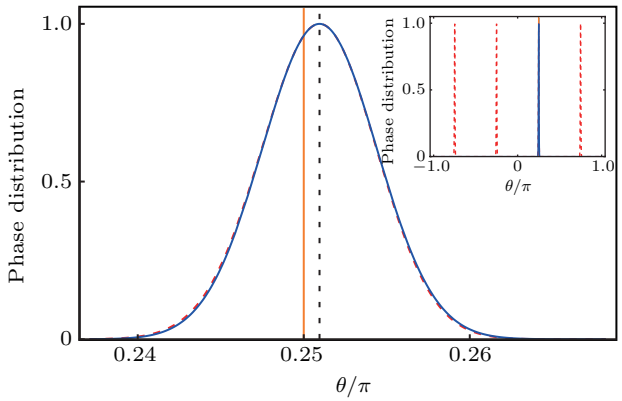


Fig. 3. Maximum likelihood estimator. For a given true value of phase shift $\theta_0 = \pi/4$, the phase distribution $\mathcal{P}(\theta|\{\mathcal{N}_\mu\})$ as a function of θ (the red dashed line), which approaches to a Gaussian (solid blue line) and hence can be used to determine the MLE θ_{est} and its variance σ (i.e, 68.3% confidence interval). The inset: four peaks of $\mathcal{P}(\theta|\{\mathcal{N}_\mu\})$ over the entire phase interval $\theta \in (-\pi, \pi)$. The occurrence number of each outcome $\mathcal{N}_\mu = \mathcal{N}_\mu(\theta_0)$ is obtained from $\mathcal{N} = 500$ random numbers.

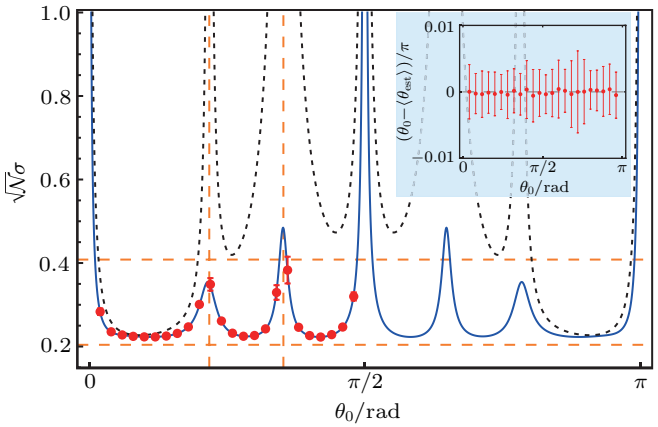


Fig. 4. For each given true value of the phase shift $\theta_0 \in (0, \pi/2)$, statistical average of $\sqrt{\mathcal{N}}\sigma$ (the solid circles) and its standard derivation (the bars), simulated by $M = 20$ replicas of $\mathcal{N} = 5000$ random numbers. Blue solid line is the CRB of the $\hat{J}_z$ measurement; and black dashed line is the CRB of the single-fringe measurement. The inset: statistical average of $(\theta_0 - \theta_{\mathrm{est}})$ as a function of θ_0 and the standard derivation. Horizontal grid lines are the shot-noise limit $1/\sqrt{N}$ and the ideal result of the QCRB $\sqrt{2}/\sqrt{N(N+2)}$ for $N = 6$. The vertical grid lines give $\theta_0 = \arctan\sqrt{2/3}$ and $\arctan 2$.

Finally, it should be mentioned that compared with other entangled states, the twin-Fock states are more robust to decoherence and give better phase estimation precision under typical experimental noise.[9] To date, small N twin-Fock states of

light have been prepared using spontaneous parametric down-conversion. Nevertheless, it is still a significant challenge to generate high photon-number states with a deterministic way. Fortunately, the deterministic preparations of atomic twin-Fock states have been proposed and demonstrated using spin-1 Bose–Einstein condensates.[20,43,44] In particular, Luo *et al.*[44] have shown that the atomic twin-Fock states can be deterministically generated by controlled quantum phase transition. These results give a renewed interest to realize phase measurements near the Heisenberg limit with large N twin-Fock states.[45]

5. Conclusion

In summary, we have investigated an optimal phase estimation protocol with the twin-Fock states as the input of a two-mode Mach–Zendner interferometer. Our analytical results indicate that the CFI of the $\hat{J}_z$ measurement is the same as that of the $\hat{J}_z^2$ measurement and both of them saturate the QFI for any true value of phase shift, i.e., $\mathcal{F}(\theta)=F_{\rm Q}=N(N+2)/2$, which leads to a global phase estimation $\delta\theta_{\rm CRB}=\delta\theta_{\rm QCRB}\simeq\sqrt{2}/N$. To demonstrated it clearly, we consider the six-particle twin-Fock state as the input and numerically simulate the $(N+1)$ occurrence probabilities of the $\hat{J}_z$ measurement, where the experimental imperfections are taken into account phenomenologically. Our results show that the maximum value of the CFI is about 20.1, approaching to the ideal result of the QFI $F_{\rm Q}=24$. Furthermore, the quantum-enhancement sensing region of the $\hat{J}_z$ measurement is about twice wider than that of the single-fringe detection, which is important to improve the global imaging quality of a quantum multiphoton microscopy.[42] Finally, we numerically simulate the phase estimation protocol using the asymptotically unbiased maximum likelihood estimator.

Appendix A: The CFI of $\hat{J}_z^2$ measurement

Due to $\hat{J}_z^2|j,\mu\rangle=\mu^2|j,\mu\rangle$, the conditional probabilities of the outcomes μ^2 (or $|\mu|$) are given by

$$p_{|\mu|}(\theta)=\begin{cases}p_0(\theta), & \mu=0,\\ p_{-\mu}(\theta)+p_\mu(\theta), & \mu>0,\end{cases}$$

which gives the CFI

$$\begin{aligned}\mathcal{F}(\theta)&=\sum_{|\mu|=0}^{j}p_{|\mu|}(\theta)\left[\frac{\partial\ln p_{|\mu|}(\theta)}{\partial\theta}\right]^2\\&=\sum_{|\mu|=0}^{j}\frac{1}{p_{|\mu|}(\theta)}\left[\frac{\partial p_{|\mu|}(\theta)}{\partial\theta}\right]^2,\end{aligned}$$

where we only consider an even number of particles $N(=2j)$. From Eq. (1), one can find that for the twin-Fock input states, the phase-dependence probabilities are symmetric about $\mu=0$, i.e., $p_{-\mu}(\theta)=p_\mu(\theta)$, which results in $p_{|\mu|}(\theta)=2p_\mu(\theta)=2[d^j_{\mu,0}(\theta)]^2$ for $\mu>0$, and therefore

$$\frac{\partial p_{|\mu|}(\theta)}{\partial\theta}=\begin{cases}2\sqrt{p_0(\theta)}\dfrac{\partial d^j_{0,0}(\theta)}{\partial\theta}, & \mu=0,\\ 4\sqrt{p_\mu(\theta)}\dfrac{\partial d^j_{\mu,0}(\theta)}{\partial\theta}, & \mu>0.\end{cases}$$

Since $\partial d^j_{\mu,0}(\theta)/\partial\theta=\langle j,\mu|\,\mathrm{e}^{-\mathrm{i}\theta\hat{J}_y}(-\mathrm{i}\hat{J}_y)|j,0\rangle\in\mathbb{R}$, we obtain

$$\begin{aligned}\mathcal{F}(\theta)&=4\left[\frac{\partial d^j_{0,0}(\theta)}{\partial\theta}\right]^2+8\sum_{\mu=1}^{+j}\left[\frac{\partial d^j_{\mu,0}(\theta)}{\partial\theta}\right]^2\\&=4\left[\frac{\partial d^j_{0,0}(\theta)}{\partial\theta}\right]^2+4\sum_{\mu=1}^{+j}\left[\frac{\partial d^j_{\mu,0}(\theta)}{\partial\theta}\right]^2\\&\quad+4\sum_{\mu=-j}^{-1}\left[\frac{\partial d^j_{-\mu,0}(\theta)}{\partial\theta}\right]^2\\&=4\sum_{\mu=-j}^{+j}\left[\frac{\partial d^j_{\mu,0}(\theta)}{\partial\theta}\right]^2\\&=4\sum_{\mu=-j}^{+j}\left[\langle j,\mu|\,\mathrm{e}^{-\mathrm{i}\theta\hat{J}_y}(-\mathrm{i}\hat{J}_y)|j,0\rangle\right]^2\\&=4\langle j,0|\hat{J}_y^2|j,0\rangle=\frac{N(N+2)}{2}=F_{\rm Q},\end{aligned}$$

where we have used the relations $d^j_{-\mu,0}(\theta)=(-1)^\mu d^j_{\mu,0}(\theta)$ and $\sum_\mu|j,\mu\rangle\langle j,\mu|=1$. For the twin-Fock input states, we show here that the CFI of the $\hat{J}_z^2$ measurement is the same with that of the $\hat{J}_z$ measurement, indicating a global phase estimation $\delta\theta_{\rm CRB}=\delta\theta_{\rm QCRB}\simeq\sqrt{2}/N$. This result remains valid in the presence of experimental imperfections, provided $p^{(\rm im)}_{-\mu}(\theta)=p^{(\rm im)}_{\mu}(\theta)$.

Appendix B: Numerical simulations

To take the experimental imperfections into account, we simply replace the occurrence probabilities by

$$p^{(\rm im)}_\mu(\theta)=\frac{h}{1+V}\left[2Vp_\mu(\theta)+(1-V)k_\mu\right],$$

where $h=0.975$ and $V=0.94$ denote the peak height and the visibility of $p^{(\rm im)}_0(\theta)$.[38] The values of k_μ are obtained by solving the relative peak heights of $\{p_\mu(\theta)\}$, i.e., $(k_0,k_{\pm1},k_{\pm2},k_{\pm3})=(1,\frac{16}{45},\frac{5}{18},\frac{5}{16})$. Next, we normalize $\{p^{(\rm im)}_\mu(\theta)\}$ to ensure $\sum_\mu p^{(\rm im)}_\mu(\theta)=1$, as Eq. (6) in the main text.

To simulate the $\hat{J}_z$ measurement, we adopt Monte Carlo method based on $\{p^{(\rm im)}_\mu(\theta)\}$ at a given phase shift θ. Specially, we first generate $\mathcal{N}$ random numbers $\{\xi_1,\xi_2,\ldots,\xi_{\mathcal{N}}\}$ and divide the interval from 0 to 1 with a discrete function $S(k)=\sum_{k'=1}^{k}p^{(\rm im)}_{k'-j-1}(\theta)$ for $k=1,2,\ldots,2j+1$, where $S(0)=0$, $S(1)=p^{(\rm im)}_{-j}(\theta)$, and $S(2j+1)=1$. When ξ_i (for $i=1,2,\ldots,\mathcal{N}$) satisfies $0\le\xi_i\le S(1)$, it can be regarded as the outcome $\mu=-j$; While for $S(k-1)<\xi_i\le S(k)$, it

is an any outcome $\mu = k - j - 1$. Therefore, we obtain the occurrence numbers of all the outcomes $\{\mathcal{N}_\mu\}$. The $\mathcal{N}$ random numbers are used to simulate a single phase measurement at the given value of phase shift θ.[39] Next, we repeat the above process for M replicas to obtain the average occurrence frequency $\langle \mathcal{N}_\mu^{(i)} \rangle_{\rm s}/\mathcal{N}$ (see the circles of Fig. 1) and its standard derivation (the bars) of each outcome after $M = 20$ replicas of $\mathcal{N} = 500$ independent measurements. Here, $\langle A^{(i)} \rangle_{\rm s} = \sum_{i=1}^{M} A^{(i)}/M$ denotes the statistical average. Finally, we obtain $\langle \mathcal{N}_\mu \rangle_{\rm s}/\mathcal{N}$ for any value of $\theta \in (-\pi, \pi)$, which is fitted by $p_\mu^{(\rm fit)}(\theta) \approx p_\mu^{(\rm im)}(\theta)$. Note that in a real experiment, the phase-dependent probabilities can be measured from the interferometer calibration.

Appendix C: The reduced CFI by coarse-graining

For a general $(N+1)$-outcome measurement with probability $\{p_\mu(\theta)\}$, denoted by $\{p_\mu\}$ for brevity, obeying $\sum_{\mu=0}^{N} p_\mu = 1$, the total CFI is given by

$$\mathcal{F} = \frac{(p_0')^2}{p_0} + \frac{(p_1')^2}{p_1} + \frac{(p_2')^2}{p_2} + \cdots + \frac{(p_N')^2}{p_N}.$$

If we consider a coarse-graining method by combining two outcomes (say $\mu = 0$ and 1) into a single outcome "$\tilde{1}$" with probability $p_{\tilde{1}} = p_0 + p_1$, then the CFI of this N-outcome measurement is

$$\tilde{F} = \frac{(p_{\tilde{1}}')^2}{p_{\tilde{1}}} + \frac{(p_2')^2}{p_2} + \cdots + \frac{(p_N')^2}{p_N}.$$

The difference of these two CFIs is given by

$$\begin{aligned} \mathcal{F} - \tilde{F} &= \frac{(p_0')^2}{p_0} + \frac{(p_1')^2}{p_1} - \frac{(p_{\tilde{1}}')^2}{p_{\tilde{1}}} \\ &= \frac{(p_0')^2}{p_0} + \frac{(p_1')^2}{p_1} - \frac{(p_0' + p_1')^2}{p_0' + p_1'} \\ &= \frac{(p_0' p_1 - p_0 p_1')^2}{p_0 p_1 (p_0' + p_1')} \geq 0, \end{aligned}$$

where the equality $\mathcal{F} = \tilde{F}$ holds if and only if

$$p_0' p_1 - p_0 p_1' = 0, \quad \frac{\partial}{\partial \theta} \ln\left(\frac{p_0}{p_1}\right) = 0,$$

i.e., if and only if p_0/p_1 is a θ-independent constant. Therefore, combining different outcomes into a single outcome either leaves the CFI invariant (if the probabilities of the outcomes being combined have the same functional dependence on up to a multiplicative constant), or strictly decreases the CFI.

Acknowledgment

We thank Prof. W. Yang for helpful discussion.

References

[1] Ma J, Wang X, Sun C P and Nori F 2011 *Phys. Rep.* **509** 89
[2] Pezzé L, Smerzi A, Oberthaler M K, Schmied R and Treutlein P 2018 *Rev. Mod. Phys.* **90** 035005
[3] Dowling J P 2008 *Contemp. Phys.* **49** 125
[4] Giovannetti V, Lloyd S and Maccone L 2004 *Science* **306** 1330
[5] Durkin G A and Dowling J P 2007 *Phys. Rev. Lett.* **99** 070801
[6] Gerry C C and Campos R A 2003 *Phys. Rev. A* **68** 025602
[7] Dorner U, Demkowicz-Dobrzanski R, Smith B J, Lundeen J S, Wasilewski W, Banaszek K and Walmsley I A 2009 *Phys. Rev. Lett.* **102** 040403
[8] Zhang Y M, Li X W, Yang W and Jin G R 2013 *Phys. Rev. A* **88** 043832
[9] Zhang Z and Duan L M 2014 *New J. Phys.* **16** 103037
[10] Holland M J and Burnett K 1993 *Phys. Rev. Lett.* **71** 1355
[11] Bollinger J J, Itano W M, Wineland D J and Heinzen D J 1996 *Phys. Rev. A* **54** R4649
[12] Gerry C C 2000 *Phys. Rev. A* **61** 043811
[13] Gerry C C, Benmoussa A and Campos R A 2002 *Phys. Rev. A* **66** 013804
[14] Gerry C C and Mimih J 2010 *Contemp. Phys.* **51** 497
[15] Anisimov P M, Raterman G M, Chiruvelli A, Plick W N, Huver S D, Lee H and Dowling J P 2010 *Phys. Rev. Lett.* **104** 103602
[16] Chiruvelli A and Lee H 2011 *J. Mod. Opt.* **58** 945
[17] Seshadreesan K P, Kim S, Dowling J P and Lee H 2013 *Phys. Rev. A* **87** 043833
[18] Kim T, Pfister O, Holland M J, Noh J and Hall J L 1998 *Phys. Rev. A* **57** 4004
[19] Zhang Y M, Li X W and Jin G R 2013 *Chin. Phys. B* **22** 114206
[20] Lücke B, Scherer M, Kruse J, Pezzé L, Deuretzbacher F, Hyllus P, Topic O, Peise J, Ertmer W, Arlt J, Santos L, Smerzi A and Klempt C 2011 *Science* **334** 773
[21] Xiang G Y, Hofmann H F and Pryde G J 2013 *Sci. Rep.* **3** 2684
[22] Helstrom C W 1976 *Quantum Detection and Estimation Theory* (New York: Academic Press)
[23] Braunstein S L and Caves C M 1994 *Phys. Rev. Lett.* **72** 3439
[24] Braunstein S L, Caves C M and Milburn G J 1996 *Ann. Phys.* **247** 135
[25] Paris M G A 2009 *In. J. Quantum Inform.* **7** 125
[26] Yurke B, McCall S L and Klauder J R 1986 *Phys. Rev. A* **33** 4033
[27] Pezzé L, Smerzi A, Khoury G, Hodelin J F and Bouwmeester D 2007 *Phys. Rev. Lett.* **99** 223602
[28] Gerry C C and Knight P L 2005 *Introductory Quantum Optics* (Cambridge: Cambridge University Press)
[29] Feng X M, Wang P, Yang W and Jin G R 2015 *Phys. Rev. E* **92** 043307
[30] Liu P, Wang P, Yang W, Jin G R and Sun C P 2017 *Phys. Rev. A* **95** 023824
[31] Liu P and Jin G R 2017 *J. Phys. A: Math. Theor.* **50** 405303
[32] Gerry C C, Campos R A and Benmoussa A 2004 *Phys. Rev. Lett.* **92** 209301
[33] Sun F W, Liu B H, Gong Y X, Huang Y F, Ou Z Y and Guo G C 2008 *Europhys. Lett.* **82** 24001
[34] Feng X M, Jin G R and Yang W 2014 *Phys. Rev. A* **90** 013807
[35] Ghirardi L, Siloi I, Bordone P, Troiani F and Paris M G A 2018 *Phys. Rev. A* **97** 012120
[36] Wang J Z, Yang Z Q, Chen A X, Yang W and Jin G R 2019 *Opt. Express* **27** 10343
[37] Xiang G Y, Higgins B L, Berry D W, Wiseman H M and Pryde G J 2010 *Nat. Photon.* **5** 43
[38] Jin G R, Yang W and Sun C P 2017 *Phys. Rev. A* **95** 013835
[39] Pezzé L and Smerzi A 2007 *Europhys. Lett.* **78** 30004
[40] Higgins B L, Berry D W, Bartlett S D, Wiseman H M and Pryde G J 2007 *Nature* **450** 393
[41] Berry D W, Higgins B L, Bartlett S D, Mitchell M W, Pryde G J and Wiseman H M 2009 *Phys. Rev. A* **80** 052114
[42] Israel Y, Rosen S and Silberberg Y 2014 *Phys. Rev. Lett.* **112** 103604
[43] Zhang Z and Duan L M 2013 *Phys. Rev. Lett.* **111** 180401
[44] Luo X Y, Zou Y Q, Wu L N, Liu Q, Han M F, Tey M K and You L 2017 *Science* **355** 620
[45] Zou Y Q, Wu L N, Liu Q, Luo X Y, Guo S F, Cao J H, Tey M K and You L 2018 *Pro. Natl. Acad. Sci. USA* **115** 6381